A CONTINUOUS, TWO-WAY FREE BOUNDARY IN THE UNSTEADY TRANSONIC SMALL DISTURBANCE EQUATIONS

ALLEN M. TESDALL

Department of Mathematics, College of Staten Island, City University of New York
Staten Island, New York 10314, United States
allen.tesdall@csi.cuny.edu

BARBARA L. KEYFITZ

Department of Mathematics, The Ohio State University
Columbus, Ohio 43210, United States
bkeyfitz@math.ohio-state.edu

Abstract.   We formulate a problem for the unsteady transonic small disturbance equations which describes a situation analogous to the reflection of a weak shock off a wedge, with the incident shock replaced by an incident rarefaction. We linearize this problem and solve it exactly, and we compute a numerical solution of the full nonlinear problem. The solution of this problem has several features in common with the solution of the weak shock reflection problem, known as Guderley Mach reflection. In both cases, a rarefaction wave reflects off a sonic line and forms a transonic shock. There is transonic coupling between the supersonic and subsonic regions across the sonic line and shock. In both situations, this sonic line/shock can be considered a free boundary in the formulation of a new type of free boundary problem which has not previously been formulated or analyzed. The free boundary problem that arises in the context of the problem considered here is, however, simpler than the free boundary problem that arises in the weak shock reflection problem.

Keywords: Free boundary problem; unsteady transonic small disturbance equations; triple point paradox; Guderley Mach reflection.

1. Introduction

When a weak incident shock wave (loosely speaking, a shock with Mach number only slightly greater than 1) reflects off a thin wedge, a reflection pattern that appears to be Mach reflection is observed, in which the incident, reflected and Mach shocks meet at a shock "triple point". However, von Neumann showed in 1943 [13] that for sufficiently weak shocks, a standard triple point configuration, consisting of three shocks and a contact discontinuity meeting in a point, is impossible. This

2   *Allen M. Tesdall and Barbara L. Keyfitz*

discrepancy is referred to as the von Neumann, or triple point, paradox. Various proposals have been put forth over the years to resolve the paradox; see [5,8] for detailed discussions. Of particular note, Guderley [7] in 1947 proposed the existence of an additional wave at the triple point, an expansion fan, to resolve the paradox in a *steady* weak shock Mach reflection (the same triple point paradox occurs in the steady case as in the unsteady one). He showed that local solutions satisfying the Rankine-Hugoniot jump conditions and consisting of three shocks, a centered expansion wave, and a contact discontinuity meeting at a point could be constructed. His resolution contained a supersonic patch at the triple point, since the flow must be supersonic for an expansion wave to occur.

Recently it has been shown that Guderley's expansion fan and supersonic patch are indeed found in a weak shock Mach reflection, although the solution is much more complicated than Guderley envisioned. In [17], numerical solutions were obtained of a problem for the unsteady transonic small disturbance equations (UTSDE) that describes the reflection of weak shocks off thin wedges. In [17], the equations were expressed in special self–similar variables, so that the area of interest – the neighborhood of the triple point – remains stationary on the numerical grid, and extreme local grid refinement can be implemented relatively easily to resolve the solution there. In a parameter range for which regular reflection is not possible, the solutions contain a structure that is similar to the one proposed by Guderley. However, instead of a single triple point, supersonic patch, and expansion wave, there is a sequence of triple points and tiny supersonic patches behind a leading triple point, with a centered expansion wave originating at each triple point. Each expansion wave reflects off the sonic line as a compression wave, becoming a reflected shock which hits the Mach stem and generates the next triple point. This structure is shown schematically in Figure 1. It was shown in [17] that the triple points with centered expansion fans are consistent with theory, and provide a resolution of the paradox. The name *Guderley Mach reflection* (GMR) was chosen for this new reflection pattern in [9].

Following the detection of Guderley Mach reflection in [17], a problem for the nonlinear wave system that is the analogue of shock reflection was studied numerically in [19]. The nonlinear wave system is a 3×3 hyperbolic system that has a characteristic structure similar to that of the compressible Euler equations, but which is not derived from them via a limit (as is the UTSDE). At a set of parameter values for which regular reflection solutions of the nonlinear wave system do not exist, a numerical solution was obtained which is remarkably similar to the solutions obtained in [17]. Again, a sequence of triple points and supersonic patches was obtained in a tiny region behind the leading triple point, with a centered expansion wave originating at each triple point. The discovery of Guderley Mach reflection in a solution of this system led to the subsequent numerical study of a shock reflection problem for the full Euler equations of gasdynamics in [20]. At a set of parameter values for which both regular and Mach reflection solutions are impossible, solutions containing Guderley Mach reflection were once again obtained. To summarize
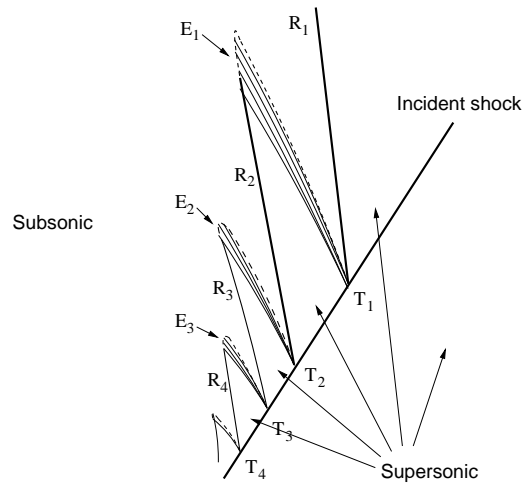
Fig. 1. A schematic diagram of Guderley Mach reflection, as obtained in [17]. The dashed line is the sonic line; flow to the right of this line is supersonic. There is a sequence of triple points, reflected shocks and centered expansion waves. The first triple point is labeled T_1, the first reflected shock is labeled R_1, and the first centered expansion wave is labeled E_1. Each reflected shock–expansion wave pair in the sequence is smaller and weaker than the one preceding it.

these recent numerical results, Guderley Mach reflection solutions have now been found in solutions of shock reflection problems for the UTSDE, the nonlinear wave system, and the full compressible Euler equations. All of the computations show that these new features are extremely small relative to the length of the Mach shock, explaining why they had not been observed before either experimentally or numerically.

On the experimental front, following the announcement of the results in [17], Skews and Ashworth modified an existing shock tube arrangement specifically to search for GMR. Their results in [15] and, more recently, the results of Skews and coauthors in [16], appear to confirm that Guderley Mach reflection occurs when a weak shock reflects off a thin wedge. A proof of existence of this structure, however, appears to be beyond our analytic techniques at the moment. In fact, we do not know even whether the sequence of patches and triple points is finite or infinite, and if it is finite, what causes its termination, and what is the nature of the solution in the final patch. Another complication is that shock waves are embedded in the sonic line, which can be considered a free boundary in the formulation of a free boundary problem. There is a transonic coupling between the subsonic and supersonic regions. The two-way coupling across the sonic line gives rise to our description of this situation as a "continuous, two-way free boundary".

Because of these difficulties, in this paper we pose a much simpler problem for the UTSDE that retains some of the features of Guderley Mach reflection. We choose initial data that correspond to a supersonic flow hitting the corner of an

4   *Allen M. Tesdall and Barbara L. Keyfitz*

expanding duct at $t = 0$. We obtain a rarefaction wave in the far field that interacts with a sonic line, producing a shock that is embedded in the sonic line. As in Guderley Mach reflection, this sonic line can be considered a free boundary, but the resulting free boundary problem is simpler than the corresponding problem for Guderley Mach reflection since there is no sequence (possibly infinite) of supersonic patches. There is an analogy, however, between the sonic line in this problem and the sonic line in a single patch in Guderley Mach reflection. In each case a rarefaction interacts with a sonic line to produce a transonic shock, and the supersonic and subsonic flows are coupled. In both cases, if one wishes to formulate and solve a free boundary problem, a degenerate hyperbolic and degenerate elliptic equation must be simultaneously solved, with data matched across the sonic line.

The problem we introduce here is more difficult than the problems studied in [3], since the location of the sonic line is unknown and has to be determined as part of the solution, along with the solution on either side of the sonic line, and because the equations on either side of the sonic line are degenerate hyperbolic/elliptic. We present a numerical solution of this problem. A proof of well-posedness remains an open issue. We do, however, linearize the problem and solve the resulting boundary value problem exactly. Our solution of the linearized problem, in fact, is what leads us to expect a transonic shock in the solution of the nonlinear problem. We subsequently show this to be the case, when we solve the nonlinear problem numerically: a transonic shock is indeed produced by the rarefaction wave/sonic line interaction.

This paper is organized as follows. In Section 2 we describe the rarefaction problem for the UTSDE. In Section 3 we formulate a linearized version of the problem and solve it exactly. In Section 4 we describe our method for solving the nonlinear problem numerically. The numerical results we obtain are presented and interpreted in Section 5.

2. The nonlinear problem

We consider an initial value problem for the unsteady transonic small disturbance equations,

$$u_t + \left(\frac{1}{2}u^2\right)_x + v_y = 0,$$
$$u_y - v_x = 0. \tag{2.1}$$

This problem consists of (2.1) together with initial data given by

$$(u, v) = \begin{cases} (0, 0) & \text{if } x > -b|y|, \\ (-1, -b) & \text{if } x < -by, \ y > 0, \\ (-1, b) & \text{if } x < by, \ y < 0. \end{cases} \tag{2.2}$$

Here $b > 0$. See Figure 2(a) for a depiction of the data.

Because the data in (2.2) is symmetric, an equivalent half-space problem in $y > 0$ is obtained by applying the no-flow boundary condition

$$v(x, 0) = 0 \tag{2.3}$$
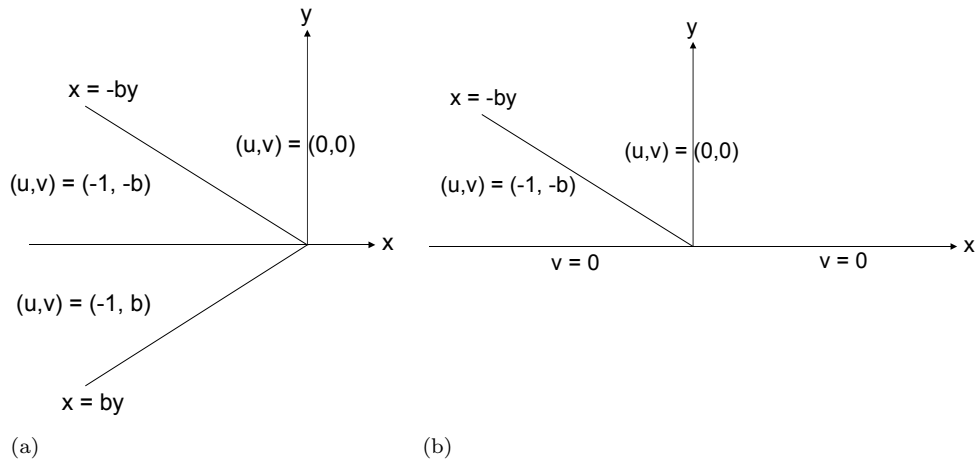
Fig. 2. In (a), initial data for the full-space problem (2.1)–(2.2), and in (b), initial data for the half-space problem consisting of (2.1)–(2.2) in $y > 0$, and (2.3).

on the axis of symmetry, $y = 0$. See Figure 2(b) for an illustration of the data for this half-space problem. The discontinuity located at $x = -by$ propagates as a rarefaction wave for $t > 0$, as we show in Section 4.1. (Equivalently, the discontinuities located at $x = \pm by$ in Figure 2(a) propagate as a pair of diverging rarefaction waves.)

The problem (2.1)–(2.2) in $y > 0$, (2.3) is self-similar, so the solution depends only on the similarity variables

$$\xi = x/t, \qquad \eta = y/t.$$

Writing (2.1) in terms of ξ and η, we get

$$-\xi u_\xi - \eta u_\eta + \left(\frac{1}{2}u^2\right)_\xi + v_\eta = 0,$$

$$u_\eta - v_\xi = 0. \tag{2.4}$$

Equation (2.4) is hyperbolic when $u < \xi + \eta^2/4$, corresponding to supersonic flow in a self-similar coordinate system, and elliptic when $u > \xi + \eta^2/4$, corresponding to subsonic flow. The equation changes type across the sonic line given by

$$\xi + \frac{\eta^2}{4} = u(\xi, \eta). \tag{2.5}$$

By abuse of notation, we will refer to the locus of transition points between $u < \xi + \eta^2/4$ and $u > \xi + \eta^2/4$ as the sonic line, whether the flow is continuous there or not. Where the rarefaction wave intersects this sonic line there will be an interaction, since rarefactions cannot be continued in the backwards time direction. In the supersonic, hyperbolic region, the inverse slopes of the (bi-)characteristic

6   *Allen M. Tesdall and Barbara L. Keyfitz*

curves of (2.4) are given by [8]

$$\frac{d\xi}{d\eta} = -\frac{1}{2}\eta \pm \sqrt{\xi + \frac{1}{4}\eta^2 - u}. \tag{2.6}$$

We refer to the characteristics as plus or minus characteristics, depending on the choice of sign in this equation.

3. The linearized problem

In order to determine the asymptotic behavior of the solution of the nonlinear problem at large distances from the rarefaction wave/sonic line interaction region, we seek the solution of a corresponding linearized problem. We linearize equation (2.1) about $u = 0$ to obtain

$$\begin{aligned} u_t + v_y &= 0, \\ u_y - v_x &= 0. \end{aligned} \tag{3.1}$$

In self-similar coordinates $\xi = x/t$, $\eta = y/t$, these equations take the form

$$\begin{aligned} -\xi u_\xi - \eta u_\eta + v_\eta &= 0, \\ u_\eta - v_\xi &= 0. \end{aligned} \tag{3.2}$$

Equation (3.2) is hyperbolic when $\xi + \eta^2/4 > 0$ and elliptic when $\xi + \eta^2/4 < 0$. The equation changes type across the sonic parabola

$$\xi + \frac{1}{4}\eta^2 = 0. \tag{3.3}$$

We again consider the piecewise constant initial data in (2.2). The jump conditions for (3.1), now derived from the linear theory of characteristics, show that the discontinuities in (2.2) propagate to the right with speed b^2. In the far field, where the two waves do not interact, so that the situation is one-dimensional, the locations of the discontinuities in self-similar variables are thus given by

$$\begin{aligned} \xi &= -b\eta + b^2, \quad \eta > \eta_0, \\ \xi &= b\eta + b^2, \quad \eta < -\eta_0, \end{aligned} \tag{3.4}$$

where $\pm\eta_0$ are the values of η where these lines meet the sonic parabola. The positions of the sonic parabola and the discontinuities are shown schematically in Figure 3. A calculation shows that $\eta_0 = 2b$. While (3.1) (like the original system (2.1)) is hyperbolic in space-time, the plane $\{t = 0\}$ is characteristic. Thus existence of a solution to (3.1), (2.2) requires conditions on Cauchy data, and uniqueness is not guaranteed. For piecewise constant data of the form (2.2), the only restriction is that u be constant across the x-axis (as is the case here). As we shall see by explicit construction, the condition that u remain bounded is sufficient to give uniqueness. We solve the problem by working in the self-similar plane, where we have already found a solution, which is piecewise constant, in the hyperbolic region. Therefore,
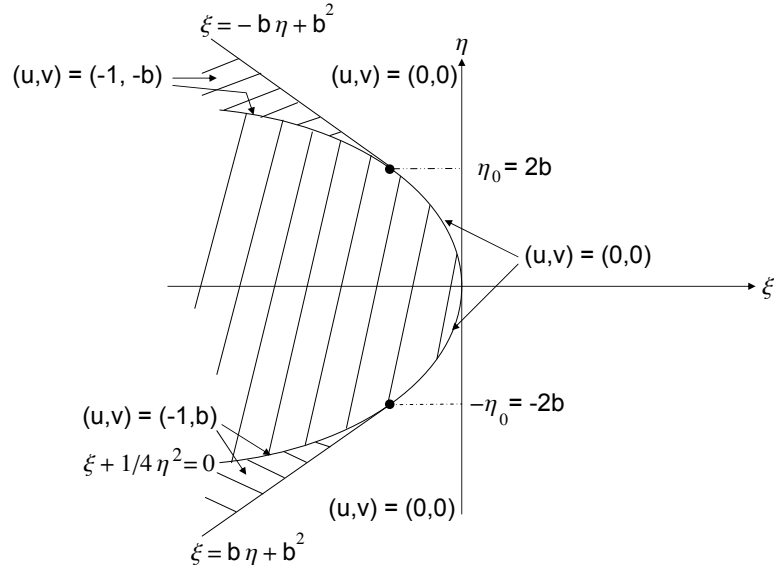
Fig. 3. An illustration of the boundary value problem for (3.2). The sonic parabola (3.3) is located at $\xi + \frac{1}{4}\eta^2 = 0$. Equation (3.2) is hyperbolic to the right of the sonic parabola, and elliptic to the left. Boundary data are indicated on the parabola.

we seek the solution of a boundary value problem for (3.2) in the region $\xi + \eta^2/4 < 0$, with boundary data given on $\xi + \eta^2/4 = 0$ by

$$(u, v) = \begin{cases} (-1, -b), & \eta > \eta_0 = 2b, \\ (0, 0), & -2b = -\eta_0 < \eta < \eta_0 = 2b, \\ (-1, b), & \eta < -\eta_0 = -2b. \end{cases} \tag{3.5}$$

We supplement this with the condition $|u| < M$ as $\xi \to -\infty$, for some M. Figure 3 illustrates the boundary conditions and domain of the boundary value problem.

   To solve this boundary value problem, we use a Busemann transformation following the method of Keller and Blank [10]. See the appendix for details. In self-similar coordinates (ξ, η), the bounded solution to (3.2), (3.5) is

$$u(\xi, \eta) = -1 + \frac{1}{\pi} \left[\tan^{-1} \frac{2\sqrt{-(\xi + \eta^2/4)}}{\eta - \eta_0} - \tan^{-1} \frac{2\sqrt{-(\xi + \eta^2/4)}}{\eta + \eta_0} \right],$$

$$v(\xi, \eta) = \frac{-\eta_0}{2\pi} \left[\tan^{-1} \frac{\eta + \eta_0}{2\sqrt{-(\xi + \eta^2/4)}} + \tan^{-1} \frac{\eta - \eta_0}{2\sqrt{-(\xi + \eta^2/4)}} \right]. \tag{3.6}$$

We note that the boundedness condition for u gave us boundedness for v also.

   Referring again to Figure 3, the complete solution of the linearized problem is given by (3.6) for $\xi + \eta^2/4 < 0$, and by the piecewise constant values for (u, v) depicted in the figure for $\xi + \eta^2/4 > 0$. This solution is continuous at the sonic line $\xi + \eta^2/4 = 0$ (with the exception of the two singular points $(-b^2, -2b)$ and $(-b^2, 2b)$,

8   *Allen M. Tesdall and Barbara L. Keyfitz*

as indicated in the figure). However, it is not differentiable: (3.6) shows that there is a square root singularity at the sonic line. Thus, the solution of the linearized problem may not extend to a continuous solution of the nonlinear problem. As the square root singularity has the structure of compression wave, we are led to expect that the nonlinear problem has a shock at the sonic line. In Section 5, we provide numerical evidence that this is in fact the case.

4. The numerical method for the nonlinear problem

The basic numerical method we use was developed in [17] specifically to solve self-similar problems for the UTSDE. However, the numerical boundary conditions we use here are quite different from those used in [17]. We outline the underlying algorithm here, and in Section 4.1 we give a full explanation of the boundary conditions. The main idea of the numerical method is the introduction of special self-similar variables,

$$r = x/t + \frac{1}{4}(y/t)^2, \qquad \theta = y/t, \qquad \tau = \log t,$$

$$\widetilde{u} = u - r, \qquad \widetilde{v} = v - \frac{1}{2}\theta u. \tag{4.1}$$

Writing (2.1) in terms of the variables in (4.1), we get

$$\widetilde{u}_\tau + \left(\frac{1}{2}\widetilde{u}^2\right)_r + \widetilde{v}_\theta + \frac{3}{2}\widetilde{u} + \frac{1}{2}r = 0,$$

$$\widetilde{u}_\theta - \widetilde{v}_r = 0. \tag{4.2}$$

Under the transformation given in (4.1) the UTSDE is unchanged except for the addition of lower-order terms, as shown in (4.2). Following the classical Cole-Murman approach, we introduce a potential $\varphi(r, \theta, \tau)$ such that

$$\widetilde{u} = \varphi_r, \qquad \widetilde{v} = \varphi_\theta, \tag{4.3}$$

and we write (4.2) in the potential form

$$\varphi_{r\tau} + \left(\frac{1}{2}\varphi_r^2\right)_r + \varphi_{\theta\theta} + \frac{3}{2}\varphi_r + \frac{1}{2}r = 0. \tag{4.4}$$

We define a logically rectangular finite-difference grid r_i in the r direction and θ_j in the θ direction, and denote an approximate solution of (4.4) by

$$\varphi_{i,j}^n \approx \varphi(r_i, \theta_j, n\Delta\tau),$$

where $\Delta\tau$ is a fixed time step. We discretize (4.4) in space and time using

$$\varphi_{i,j}^{n+1} - \Delta r_{i+1/2}\Delta\tau \left(\frac{\frac{\varphi_{i,j+1}-\varphi_{i,j}}{\Delta\theta_{j+1/2}} - \frac{\varphi_{i,j}-\varphi_{i,j-1}}{\Delta\theta_{j-1/2}}}{\Delta\theta_j}\right)^{n+1} + \frac{3}{2}\Delta\tau\varphi_{i,j}^{n+1}$$

$$= \varphi_{i+1,j}^{n+1} - \varphi_{i+1,j}^n + \varphi_{i,j}^n + \Delta\tau\left(F(\widetilde{u}_{i+1/2,j}, \widetilde{u}_{i+3/2,j})^n - F(\widetilde{u}_{i-1/2,j}, \widetilde{u}_{i+1/2,j})^n\right)$$

$$+ \frac{3}{2}\Delta\tau\varphi_{i+1,j}^{n+1} + \frac{1}{2}\Delta\tau\Delta r_{i+1/2}\, r_i. \tag{4.5}$$
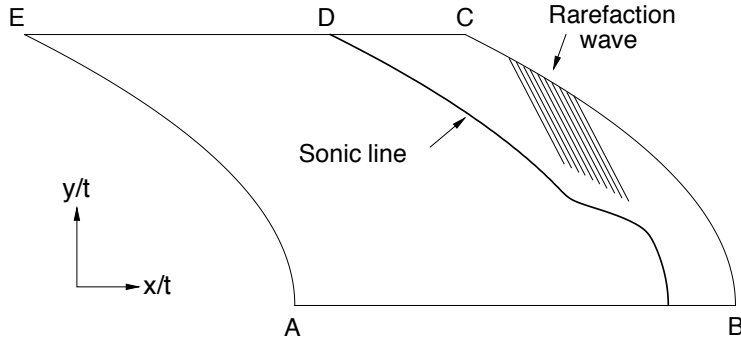
Fig. 4. A schematic diagram of the computational domain. AB is the wall and $BCDEA$ is the numerical boundary. In the region to the right of the sonic line, the flow is supersonic, and to the left it is subsonic.

Here, F is a second order minmod-limited numerical flux function, and

$$\widetilde{u}_{i-1/2,j} = \frac{\varphi_{i,j} - \varphi_{i-1,j}}{\Delta r_{i-1/2}}.$$

Additional nomenclature used in (4.5) is quite standard. For example, $r_{i+1} = r_i + \Delta r_{i+1/2}$, and $\Delta r_i = \frac{1}{2}(\Delta r_{i-1/2} + \Delta r_{i+1/2})$, with similar definitions applying in the θ-direction. We evolve a solution of (4.5) forward in pseudo-time τ until it converges to a steady state, using semi-implicit time marching. See [17] for further details of the numerical algorithm.

4.1. *Boundary conditions*

For computational efficiency, we solve the half-space problem (2.1)–(2.2) in $y > 0$, together with (2.3), since this requires only half as many grid points as the full-space problem (2.1)–(2.2) for the same numerical resolution. We computed solutions on the finite computational domain shown schematically in Figure 4. The left and right boundaries of the computational domain are curved because of the use of the parabolic coordinates in (4.1).

On the wall boundary AB we impose the physical no-flow condition (2.3), which implies that $\varphi_\theta = 0$. In addition, we require numerical boundary conditions on the outer computational boundaries, which we determine as follows.

As noted in Section 2, the discontinuity in Figure 2(b) propagates as a rarefaction wave. This rarefaction enters the computational domain through the right boundary BC, as indicated in Figure 4. By solving a one-dimensional Riemann problem, we find that the rarefaction wave solution is given by

$$(u,v) = \begin{cases} (-1,-b) & \text{if } x + by < (b^2-1)t, \\ \big((x+by-b^2t)/t, b(x+by-b^2t)/t)\big) & \text{if } (b^2-1)t \le x+by \le b^2t, \quad (4.6) \\ (0,0) & \text{if } x + by > b^2t. \end{cases}$$

10   *Allen M. Tesdall and Barbara L. Keyfitz*
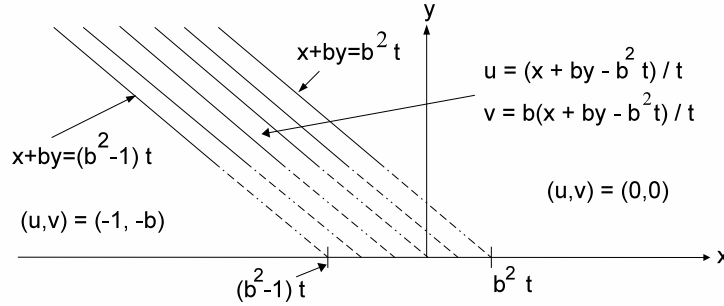
Fig. 5. The far field solution. The front of the rarefaction, located at $x + by = b^2t$, propagates to the right for $t > 0$. The rear of the rarefaction either propagates to the right, is stationary at $x = -by$, or propagates to the left, depending on the value of b. The dashed lines emphasize that this solution is valid only sufficiently far from the origin.

This solution is illustrated in Figure 5.

On the right boundary BC, we impose Dirichlet data corresponding to the rarefaction solution in (4.6). The location of the propagating expansion wave is given by

$$(b^2 - 1)t \le x + by \le b^2t. \tag{4.7}$$

Using (4.1) in (4.7), we find that the location of the rarefaction in terms of the transformed self-similar coordinates r and θ is given by

$$-b\theta + \frac{1}{4}\theta^2 + b^2 - 1 \le r \le -b\theta + \frac{1}{4}\theta^2 + b^2.$$

Thus, the rarefaction wave is bounded by parabolas with respect to the transformed coordinates, instead of by straight lines. Ahead of the rarefaction we have $(u, v) = (0, 0)$, behind it we have $(u, v) = (-1, -b)$, and inside the wave the solution (u, v) is given by the middle expression in (4.6). So, using (4.1), (4.3), and the requirement that the potential is continuous across the rarefaction, we find that the potential for the far field rarefaction solution is

$$\varphi(r, \theta) = \begin{cases} -\frac{1}{2}r^2, & \text{if } r > -b\theta + \frac{1}{4}\theta^2 + b^2, \\ \{\frac{1}{32}\theta^4 - \frac{1}{4}b\theta^3 + (\frac{3}{4}b^2 - \frac{1}{4}r)\theta^2 & \text{if } -b\theta + \frac{1}{4}\theta^2 + b^2 - 1 < r \\ \quad +(br - b^3)\theta - b^2r + \frac{b^4}{2}\}, & \quad < -b\theta + \frac{1}{4}\theta^2 + b^2, \\ -r - \frac{1}{2}r^2 - b\theta + \frac{1}{4}\theta^2 + b^2 - \frac{1}{2}, & \text{if } r < -b\theta + \frac{1}{4}\theta^2 + b^2 - 1. \end{cases} \tag{4.8}$$

We impose (4.8) as a boundary condition for (4.4) on BC.

The asymptotic behavior of the solution of the nonlinear problem at large distances from the origin is assumed to be given by the solution of the linearized problem in (3.6). This corresponds to assuming that u tends to the constant value -1 as $\xi \to -\infty$. We use this solution to formulate a numerical boundary condition

on the subsonic boundary DEA. In terms of the self-similar variables in (4.1), the linearized solution for $\widetilde{u} = \varphi_r$ behind the sonic line located at $r = -1$ is

$$\varphi_r = -1 - r + \frac{1}{\pi}\left[\tan^{-1}\left(\frac{2\sqrt{-(r+1)}}{\theta - 2b}\right) - \tan^{-1}\left(\frac{2\sqrt{-(r+1)}}{\theta + 2b}\right)\right], \quad r < -1.$$

We write this equation as $\varphi_r = f(r, \theta)$, and discretize it using

$$\frac{\varphi_{i+1,j} - \varphi_{i,j}}{\Delta r_{i+1/2}} = f(r_{i+1/2}, \theta_j). \tag{4.9}$$

We impose (4.9) as a Neumann condition on the left boundary EA. On the top boundary CDE, we impose (4.9) when $r < -1$, corresponding to boundary segment DE. For $r > -1$, corresponding to the segment CD, we impose the Dirichlet condition (4.8). The exact location of the shock produced by the rarefaction/sonic line interaction is slightly different from $r = -1$, where we switch the numerical boundary conditions, and the exact solution differs slightly from the linearized solution, but we found that the disturbance originating from the top boundary is extremely small. On the other hand, we found that the use of (4.9) as a subsonic boundary condition was crucial. The use of simpler boundary conditions such as extrapolation, which are well understood in the computation of solutions of the usual time-dependent unsteady transonic small disturbance equations (see, for example, [6]) result in unacceptably large errors in the solution in the subsonic portion of the flowfield. This is not surprising, since in the subsonic region (2.4) is elliptic, and errors produced at the boundaries influence the entire region.

5. Numerical results

We computed a numerical solution of (2.1)–(2.2) in $y > 0$, and (2.3) for b equal to 0.5. Figures 6(a) and (b) show u- and v-contour plots, respectively, of the global solution as functions of $(x/t, y/t)$. The state ahead of the rarefaction is constant, with $(u, v) = (0, 0)$, and there is a constant region of flow behind the rarefaction, with $(u, v) = (-1, -0.5)$. There is a shock behind the rarefaction wave, as indicated (this is especially evident in the plot in (b)). In order to show this shock and other solution features more clearly, in Figure 7 we show surface mesh plots of u and v. These plots have been rotated in relation to the plots presented in Figure 6, as indicated, so that the shock is more clearly visible. The strength of the rarefaction wave, as measured by the change in u from the state ahead of it to the state behind it, is -1. The plot in Figure 7(a) shows that the rarefaction wave is much stronger than the shock. From the numerical data, the shock forms at $(x/t, y/t) \approx (-1.5, 1.6)$. The shock strength, as measured by the jump $[u]$ in u, increases initially as it moves away from the formation point, then decreases, approaching zero as $y/t \to +\infty$. The shock attains its maximum strength $[u]_{max} \approx 0.12$ at $(x/t, y/t) \approx (-1.7, 1.8)$. In order to capture the shock more sharply, we used local grid refinement in the area of the shock formation point. In the plots shown in Figure 7, however, we have

12   *Allen M. Tesdall and Barbara L. Keyfitz*
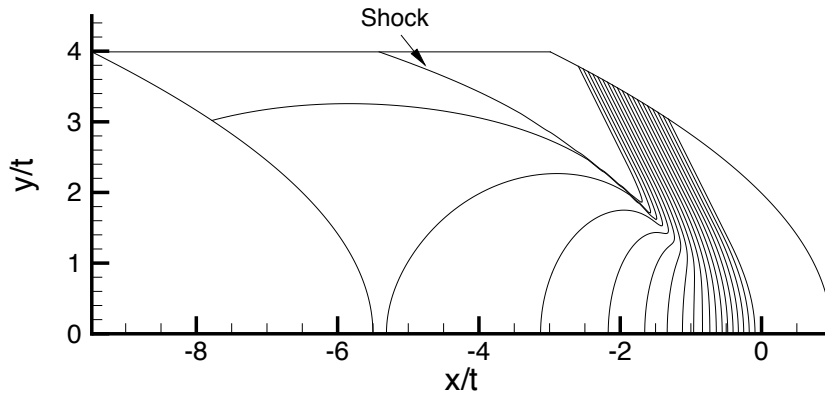
(**a**) *u*-velocity
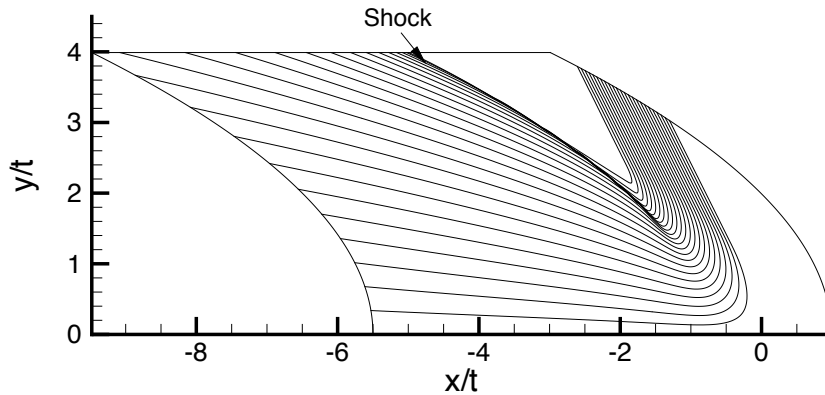
(**b**) *v*-velocity

Fig. 6. Contour plots of velocity over the full numerical domain, for $b = 0.5$. The rarefaction wave enters the computational domain through the curved right boundary. The *u*-contour spacing is 0.02 in (a) and the *v*-contour spacing is 0.05 in (b). Local grid refinement was used in the area of the shock formation point, with $\Delta\xi = \Delta\eta = 6.25 \times 10^{-5}$ in the refined grid area.

displayed a solution computed on a uniform grid, and have displayed only a portion of the mesh points, to avoid obscuring the shock area.

In Figure 8(a) we show *u*-contours and the numerically computed location of the sonic line (2.5), in order to illustrate the regions of supersonic and subsonic flow in our solution. The sonic line runs down the shock, through the rarefaction wave, and down to the wall, as indicated. In the region to the right of the sonic line $u < \xi + \eta^2/4$, so the flow there is supersonic, and to the left $u > \xi + \eta^2/4$, and the flow is subsonic. In Figure 9 we present velocity profiles taken at several vertical cuts through the shock, and the locations of these cuts are indicated by the short vertical line segments through the sonic line in Figure 8(a).

A Continuous, Two-way Free Boundary in the Unsteady TSD Equations   13

(a)

(b)
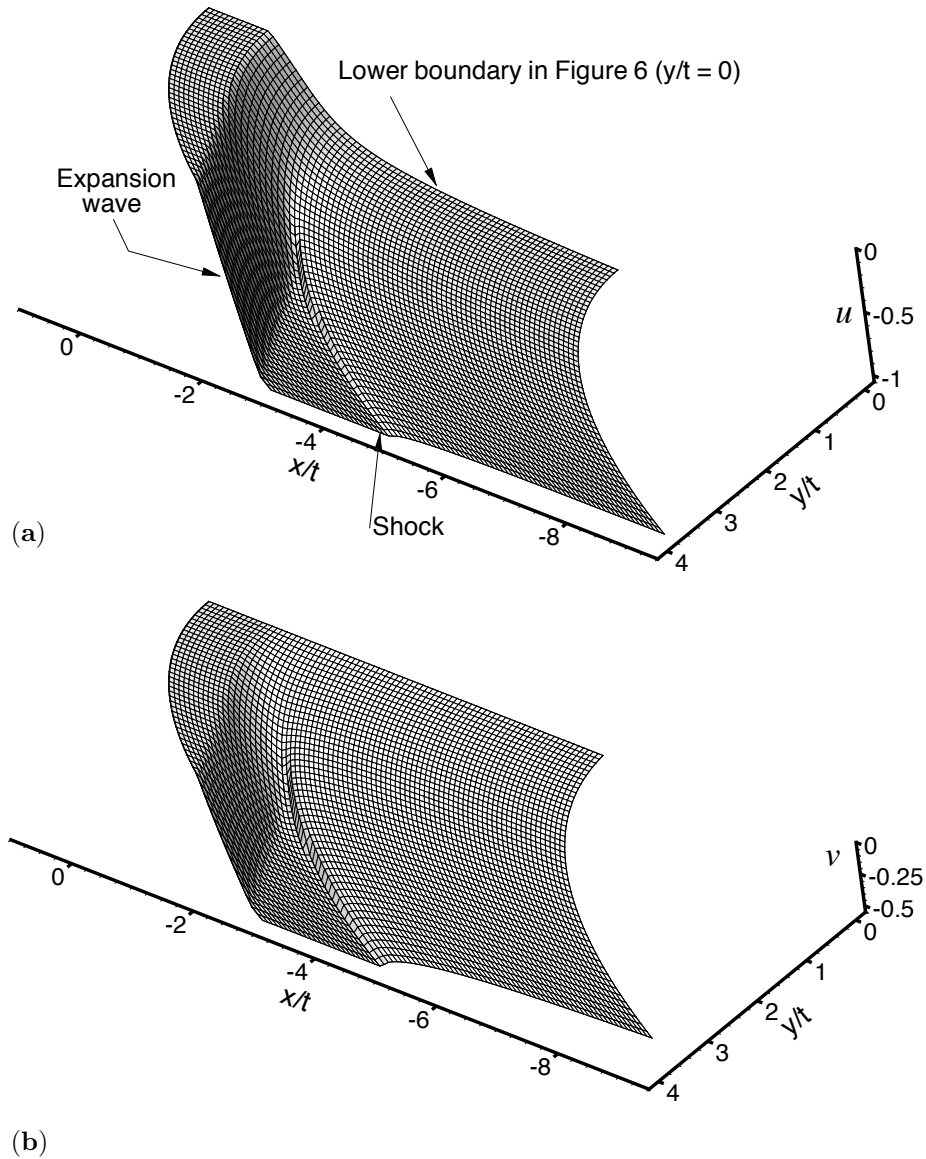
Fig. 7. A surface mesh plot of u in (a), and v in (b), for $b = 0.5$, rotated so that the bottom boundary in Figure 6 is at the top of each surface plot. The state ahead of (to the left of, in this view) the expansion wave is $(u, v) = (0, 0)$, and the state behind it is $(u, v) = (-1, -0.5)$. The solution displayed was computed using a uniform grid with $\Delta\xi = \Delta\eta = 2.5 \times 10^{-3}$. Only a portion of the numerical grid points are displayed, so that the shock appears less sharp than it actually is.

In Figure 8(b) we focus on the sonic line (2.5) that is depicted in the plot in (a), in order to illustrate its location. For constant states, the sonic line, $\xi + \eta^2/4 = u$, is a parabola in the (ξ, η)-plane, and two sonic parabolas are of interest. Ahead of

14   *Allen M. Tesdall and Barbara L. Keyfitz*

(a)

(b)
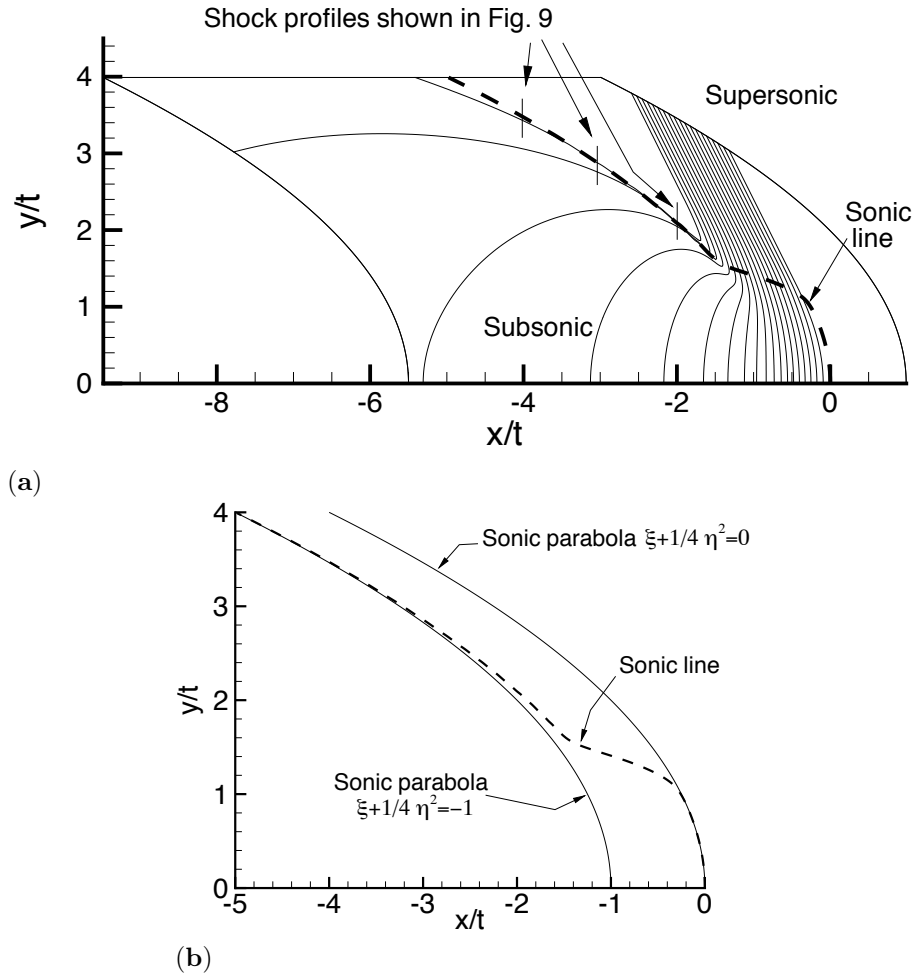
Fig. 8. In (a), a contour plot of u with the sonic (dashed) line superimposed; see Figure 9 for shock velocity profiles at the indicated cuts. The u-contours are plotted at the same levels as in Figure 6(a). The plot in (b) illustrates the location of the sonic (dashed) line, relating this to the locations of the sonic parabolas for the states ahead of and behind the rarefaction.

the rarefaction, $u = 0$, and so equation (2.4) changes type across the sonic parabola $\xi + \eta^2/4 = 0$. This is illustrated in Figure 8(b), which shows that the forward portion of the sonic line, which corresponds to the flow ahead of the rarefaction wave, appears to coincide with the curve $\xi + \eta^2/4 = 0$. Behind the rarefaction wave $u = -1$, and if the flow were continuous there, then equation (2.4) would change type across the sonic parabola $\xi + \eta^2/4 = -1$. As we have seen, however, there is a shock at the sonic line behind the rarefaction, and although it is weak it moves at greater than sonic velocity. This is also illustrated in Figure 8(b), which shows that the portion of the sonic line corresponding to the flow behind the rarefaction is
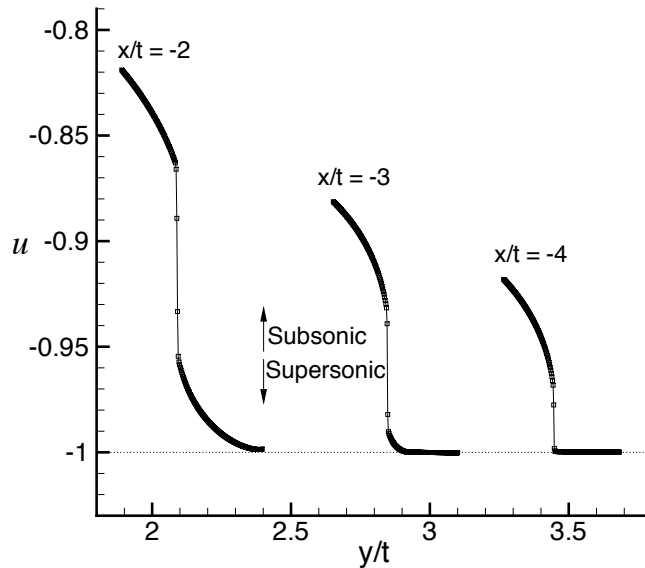
Fig. 9. Shock profiles of u-velocity taken across the shock at different x/t locations; these locations are indicated in Figure 8(a). The dotted line represents the constant supersonic state behind the rarefaction. The high-resolution numerical method captures the shock in approximately two mesh points, as indicated.

located close to, but slightly ahead of, the sonic parabola $\xi + \eta^2/4 = -1$. The sonic line appears to asymptotically approach the location $\xi + \eta^2/4 = -1$ as $y/t \to \infty$. As it crosses the rarefaction wave, the sonic line appears to bend smoothly to connect the two (approximately) parabolic portions.

In Figure 9, we show cross sections of u (referred to as shock profiles) taken at three different vertical cuts through the shock, from the numerical data. The locations and lengths of these cuts are indicated by the short vertical line segments depicted in Figure 8(a): each cut has length $y/t \approx 0.5$, and the cuts are taken through the shock at the locations $x/t = -4$, $x/t = -3$, and $x/t = -2$. Proceeding vertically upwards along one of the line segments in Figure 8(a) and measuring u (that is, measuring u while y/t increases and x/t is held constant) corresponds to moving from left to right along the corresponding shock profile in Figure 9. Hence, in moving from left to right along a given shock profile in Figure 9, the transition is from subsonic to supersonic flow, as indicated in the figure. For small values of y/t in a given shock profile, u is non-constant, corresponding to the subsonic region below the shock in Figure 8(a). As y/t increases in a profile, u jumps approximately discontinuously (note the mesh points "inside" the jump), corresponding to crossing the shock. At sufficiently large values of y/t in a profile, u reaches a constant value of -1, corresponding to the constant supersonic state with $u = -1$ behind the rarefaction. The shock strength $[u] \approx 0.095$ at $x/t = -2$, and decreases as x/t

decreases, as shown. We note that in its depiction here, the numerical shock appears steeper than it did in Figure 7. This is due to the fact that, in Figure 7, only a portion of the data points were shown.

The preceding discussion of the shock has made no mention of the point in the finite plane where the shock begins. The exact location of this point is difficult to capture numerically, but it appears to be very close to or at the sonic line. Careful numerical calculations [18] show that the shock forms strictly inside the supersonic region.

5.1. *Interpretation of the Numerical Results*

While it is standard that, in this as in any elliptic problem, the boundary conditions influence the entire region, the nature of the causality in the hyperbolic region of this problem is less obvious. The numerical results help to shed some light on the situation.

As u is not constant on the sonic line, the (bi-)characteristic curves intersect this line transversally. Recall that in a planar (straight line) rarefaction wave, one characteristic direction lies along the u-contours. Recall in addition, that through any point (ξ_0, η_0) in the hyperbolic region pass two bicharacteristic curves; their directions are tangent to the parabola $\xi + \eta^2/4 = u(\xi_0, \eta_0)$, as in (2.6). The forward time direction is toward the parabola. If we take as given the structure of the solution illustrated in the simulations, then the key point is that the rarefaction wave is reflected at the sonic line. The reflected waves affect the solution, so that near the sonic line, the rarefaction is no longer planar (in fact, technically it is no longer a rarefaction – that is, no longer a simple wave). The outer boundary of the region influenced by the interaction with the sonic line is given by a curve Γ: It is the integral curve through $P_0 = (b^2, 2b)$ of the direction field given by the minus characteristic at each point. The curve Γ continues (as a straight line) beyond the rarefaction, terminating at the shock. See [11, Example 5.1]. Figure 10(a)-(b) shows the numerically computed characteristic vector fields of the solution inside the region bounded by the sonic line and Γ. Thus, the interaction between super- and subsonic points takes place in three regimes along the sonic line, separated from each other by a priori undetermined points:

(i) Near the nose of the parabolic subsonic region, a sonic line across which the flow in continuous, with the flows on either side matched by the equation $u(\xi, \eta) = \xi + \eta^2/4$ and by the continuity of v. The shock, as mentioned, forms inside the hyperbolic region but becomes transonic at a point P_1 quite near its formation point. The sketch in Figure 11 greatly exaggerates the distance from the shock formation point to P_1.

(ii) Between P_1 and the point P_2 where the shock intersects Γ, the shock is transonic. The super- and subsonic regions are coupled by the two Rankine-Hugoniot conditions. However, the shock itself is a (downstream) spacelike curve for the supersonic flow, which is determined by upstream conditions.

(a)   (b)

(c)
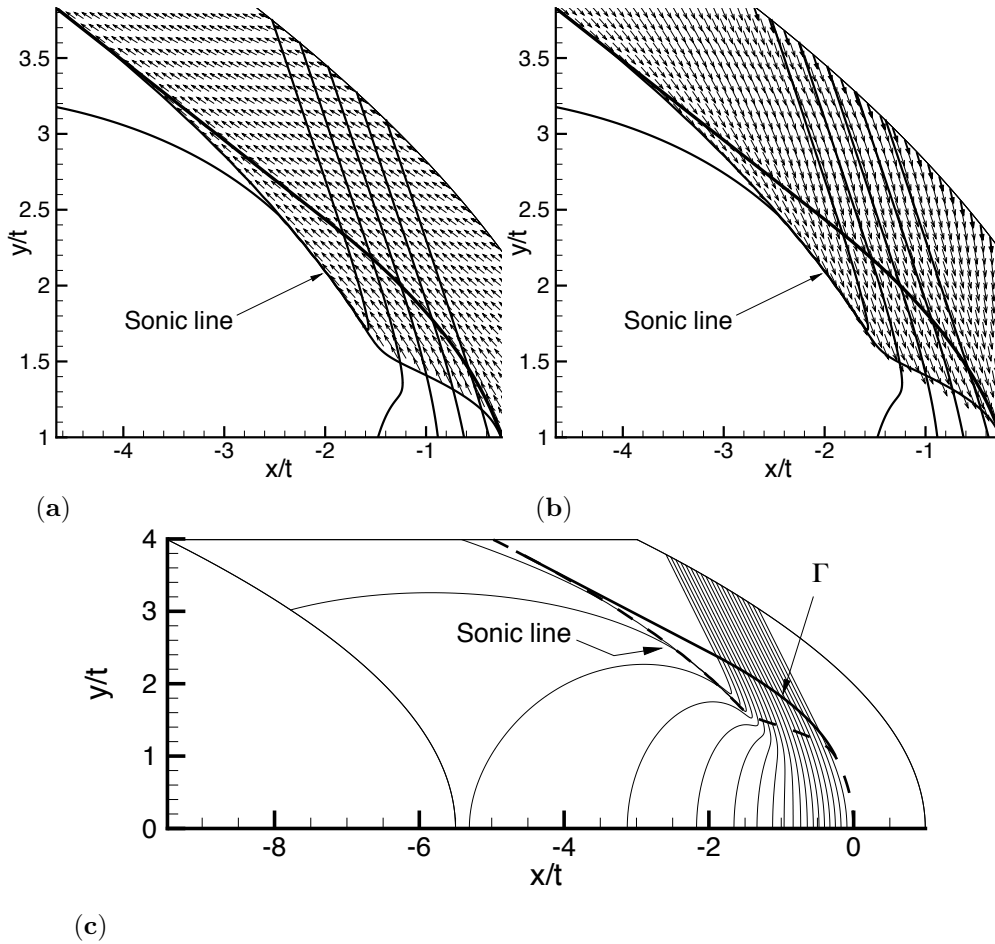
Fig. 10. The minus (a) and plus (b) characteristic vector fields in the region bounded by the curve Γ (heavy line) and the sonic line. Coarsely spaced u-contours indicate the location of the rarefaction. The direction of propagation along the self-similar characteristics is in the direction of decreasing $\xi + \eta^2/4$. The plot in (c) gives an overall impression of this region (the sonic line is the dashed line).

In particular, the subsonic flow does influence the supersonic solution locally here, but only indirectly via the coupling in (i).

(iii) Beyond P_2 we have a standard transonic shock of the type analysed in [1] or [2]. Here the supersonic state locally is determined (and constant).

The real "continuous, two-way free boundary", then, is confined to the interval of the free boundary between P_0 and P_1. Analysis of the problem is complicated by the need to include shock formation and by the fact that the subsonic region extends well beyond the segment $P_0 P_1$ – it is, in fact, unbounded for the UTSD equation. (Even for the Nonlinear Wave System of [11], where the subsonic region is bounded,
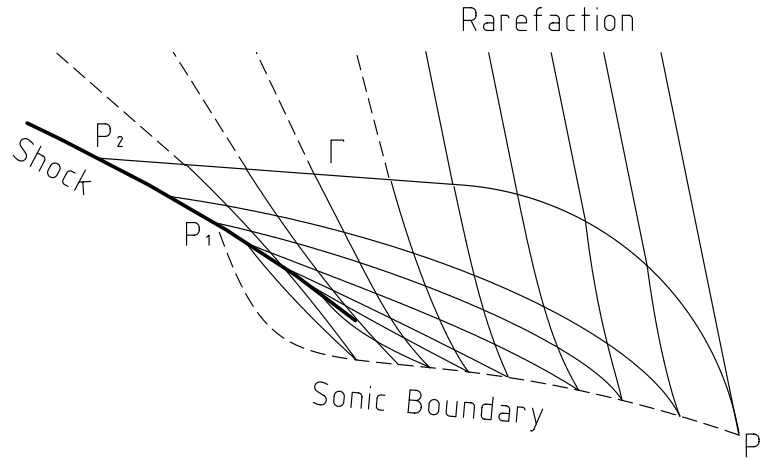
Fig. 11. A schematic diagram of the region shown in Figure 10, illustrating the characteristic and shock structure (as determined by the numerical solution), and the domain of the free boundary problem. The shock begins inside the supersonic region, as shown.

the problem is coupled to the shock part of the free boundary.) A model for the coupling in (i) is considered in [12].

A possible approach to solving this free boundary problem is mentioned in [4].

Finally, in Figure 12 we illustrate the close relationship between the problem for the reflecting rarefaction and the problem for Guderley Mach reflection, which was noted in Section 1. The plot in Figure 12(a) shows an enlargement of the solution depicted in Figure 8 in a region centered about the shock formation point. The plot in (b) shows a solution of the weak shock reflection problem for the UTSDE obtained in [17]. Both plots show v-contours and the numerically computed location of the sonic line. In (b), a single supersonic patch (and part of a second patch) in the sequence of patches comprising GMR are shown. There is a centered expansion wave, generated at the intersection of three shocks. This expansion wave reflects off the sonic line into a compression wave which steepens into a shock, as indicated. Similarly, in the plot in (a) an expansion wave reflects off a sonic line and forms a shock. Unlike GMR, in the solution of the rarefaction problem there is no fine structure in the neighborhood of the rarefaction/sonic line interaction: there is a single shock and hence a single shock formation point, and no sequence of supersonic patches and shocks.

The structure of the solution of the problem considered here, including the possible existence of shocks, was a priori unknown. Based on our solution of the linearized problem in Section 3, we conjectured that the solution of the nonlinear problem has a shock at the sonic line. The numerical results we have presented appear to confirm the existence of this shock, and in addition (see [18]) show that

(a) The nonlinear problem

(b) GMR
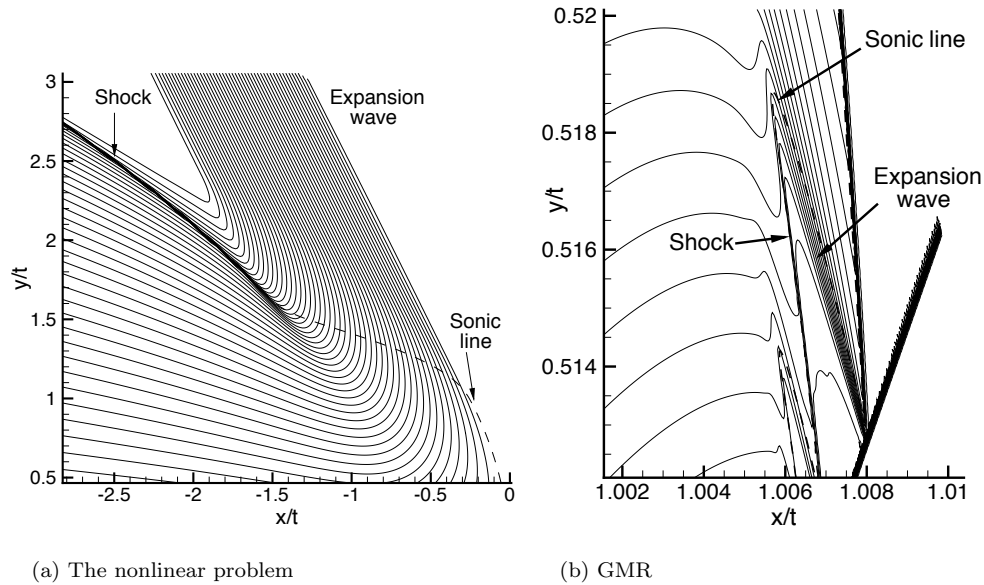
Fig. 12. A comparison of the reflecting rarefaction problem and Guderley Mach reflection. The plots show v-velocity contours from numerical solutions of the reflecting rarefaction problem in (a), and for GMR in (b). The region shown in (b) contains a single supersonic patch from the multiple patch GMR structure; the tip of the next patch is visible to the left of this patch, and the shock from the preceding patch is to its right. In both (a) and (b), the solution is supersonic to the right of the sonic line, and subsonic to the left.

the shock forms inside the supersonic region. In the formulation of a free boundary problem on the domain shown in Figure 11, therefore, part of the free boundary is continuous (the continuous part of the sonic line) and the remainder consists of a transonic shock. Moreover, as we showed in Figure 8(b), we can explain the location of the sonic line in terms of the sonic parabolas for the constant states ahead of and behind the rarefaction. Therefore, the sonic line has the structure we predicted for it: it contains an embedded shock, and it is located approximately where we expect it to be.

Acknowledgments

Appendix A. Solution of the boundary value problem

Here, we solve the linear boundary value problem (3.2), (3.5). We make a change of variables to the Busemann coordinates

$$X = 2\sqrt{-(\xi + \eta^2/4)}, \quad Y = \eta.$$

After a calculation, equation (3.2) can be written in these coordinates as

$$\frac{1}{2}(Xu_X + Yu_Y) - v_Y = 0,$$
$$\frac{1}{2}(-Yu_X + Xu_Y) + v_X = 0. \tag{A.1}$$

Differentiating the first equation with respect to X and the second with respect to Y, and adding, we obtain

$$u_{XX} + u_{YY} = 0. \tag{A.2}$$

Similarly, by reversing the differentiation we find that $v_{XX} + v_{YY} = 0$.

The sonic parabola $\xi + \eta^2/4 = 0$ is mapped by the Busemann transformation to the Y-axis, and the region $\xi + \eta^2/4 < 0$ interior to the parabola is mapped to the right half-plane in (X, Y)-space, as indicated in Figure 13. Therefore, we look for functions u and v that are harmonic in $X > 0$, and take on the boundary values (on $X = 0$) indicated in (3.5). The procedure that we will follow is to solve a Dirichlet problem for u, and then to obtain v from the solution by integration. The Dirichlet problem consists of (A.2) together with the boundary conditions

$$u(0, Y) = \begin{cases} -1, & Y > Y_0 = 2b, \\ 0, & -2b = -Y_0 < Y < Y_0 = 2b, \\ -1, & Y < -Y_0 = -2b. \end{cases} \tag{A.3}$$

The Dirichlet problem is depicted schematically in Figure 13.

The bounded solution to (A.2)-(A.3) can be obtained using standard methods from elementary complex analysis; see, for example, [14]. The solution is

$$u(X, Y) = -1 + \frac{1}{\pi}\left[\tan^{-1}\frac{X}{Y - Y_0} - \tan^{-1}\frac{X}{Y + Y_0}\right]. \tag{A.4}$$

Next we obtain $v(X, Y)$. From (A.1) we have

$$v_Y = \frac{1}{2}(Xu_X + Yu_Y), \tag{A.5}$$
$$v_X = -\frac{1}{2}(-Yu_X + Xu_Y).$$

Integrating v in X from the point $(0, 0)$, and using the second equation in (A.5),
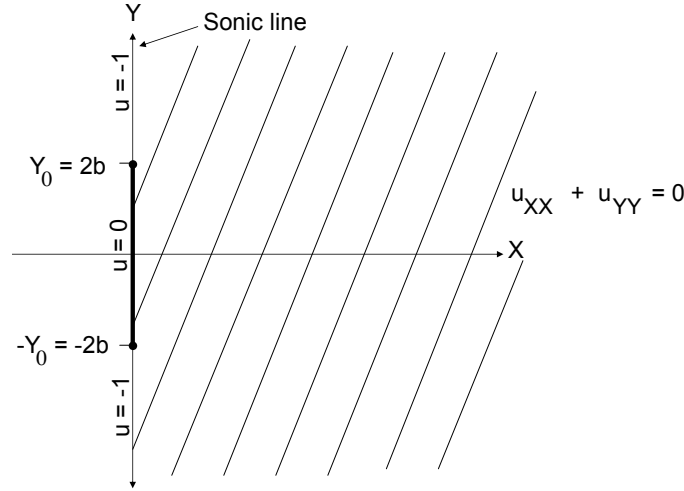
Fig. 13. Illustration of the Dirichlet problem for u. Boundary conditions are given on $X = 0$.

we calculate that

$$v(X,0) = v(0,0) + \int_0^X v_X(X,0)\,dX$$

$$= v(0,0) - \frac{1}{2} \int_0^X X u_Y(X,0)\,dX$$

$$= v(0,0) - \frac{1}{2\pi} \int_0^X \left(\frac{X^2}{X^2 + (-Y_0)^2} - \frac{X^2}{X^2 + (Y_0)^2} \right) dX.$$

In the last expression on the right, we have computed u_Y, and evaluated it at $Y = 0$, from our solution for u in (A.4). Since the integrals cancel, we obtain

$$v(X,0) = v(0,0) = 0.$$

Now we use the first equation in (A.5) to integrate in Y. We calculate that

$$v(X,Y) = v(X,0) + \int_0^Y v_Y(X,Y)\,dY$$

$$= 0 + \int_0^Y \frac{1}{2}(X u_X + Y u_Y)\,dY.$$

Again we compute u_X and u_Y from (A.4), and substitute into the integral on the right. After another calculation, we obtain

$$v(X,Y) = \frac{-Y_0}{2\pi} \left[\tan^{-1} \frac{Y + Y_0}{X} + \tan^{-1} \frac{Y - Y_0}{X} \right]. \tag{A.6}$$

Finally, we return to the self-similar coordinates (ξ, η). The solution of the boundary value problem is given by (3.6).

References

[1] S. ČANIĆ, B. L. KEYFITZ, AND E. H. KIM, *Free boundary problems for the unsteady transonic small disturbance equation: Transonic regular reflection*, Meth. Appl. Anal., 7 (2000), 313–336.

[2] S. ČANIĆ, B. L. KEYFITZ, AND E. H. KIM, *A free boundary problem for a quasilinear degenerate elliptic equation: Regular reflection of weak shocks*, Comm. Pure Appl. Math. LV (2002), 71–92.

[3] S. ČANIĆ, B. L. KEYFITZ, AND E. H. KIM, *Free boundary problems for nonlinear wave systems: Mach stems for interacting shocks,* SIAM J. Math. Anal., 37 (2005), 1947–1977.

[4] J. CHEN, C. CHRISTOFOROU, K. JEGDIC, *Rarefaction wave interaction for the unsteady transonic small disturbance equations*, Proceedings of The 15th American Conference on Applied Mathematics, ISBN: 978-960-474-071-0, ISSN: 1790-5117, University of Houston - Downtown, Houston, TX (2009), 211–216.

[5] P. COLELLA AND L. F. HENDERSON, *The von Neumann paradox for the diffraction of weak shock waves*, J. Fluid Mech., 213 (1990), 71–94.

[6] B. ENGQUIST AND A. MAJDA, *Absorbing boundary conditions for the numerical evaluation of waves*, Math. of Comp., 31 (1977), 629–651.

[7] K. G. GUDERLEY, *Considerations of the structure of mixed subsonic-supersonic flow patterns*, Air Materiel Command Tech. Report, F-TR-2168-ND, ATI No. 22780, GS-AAF-Wright Field No. 39, U.S. Wright-Patterson Air Force Base, Dayton, Ohio, October 1947.

[8] J. K. HUNTER AND M. BRIO, *Weak shock reflection*, J. Fluid Mech., 410 (2000), 235–261.

[9] J. K. HUNTER AND A. M. TESDALL, *Weak shock reflection.* In "A Celebration of Mathematical Modeling: The Joseph B. Keller Anniversary Volume," eds. D. Givoli, M. Grote, and G. Papanicolaou, Kluwer Academic Press, New York (2004), pp. 93–112.

[10] J. B. KELLER AND A. BLANK, *Diffraction and reflection of pulses by wedges and corners*, Comm. Pure Appl. Math., 4 (1951), 75–94.

[11] B. L. KEYFITZ, *Self-similar solutions of two-dimensional conservation laws*, J. Hyp. Diff. Eqns., 1 (2004), 445–492.

[12] B. L. KEYFITZ, A. M. TESDALL, K. R. PAYNE, AND N. I. POPIVANOV, *The sonic line as a free boundary*, in preparation.

[13] J. VON NEUMANN, *Collected Works*, Vol. 6, Pergamon Press, New York, 1963.

[14] E. SAFF AND A. D. SNIDER, *Fundamentals of Complex Analysis with Applications to Engineering and Science*, Prentice-Hall, 2003.

[15] B. SKEWS AND J. ASHWORTH, *The physical nature of weak shock wave reflection*, J. Fluid Mech., 542 (2005), 105–114.

[16] B. SKEWS, G. LI, AND R. PATON, *Experiments on Guderley Mach reflection*, Shock Waves, 19 (2009), 95–102.

[17] A. M. TESDALL AND J. K. HUNTER, *Self-similar solutions for weak shock reflection*, SIAM J. Appl. Math., 63 (2002), 42–61.

[18] A. M. TESDALL, *High-resolution solutions for shock formation in transonic flow,* in preparation.

[19] A. M. TESDALL, R. SANDERS, AND B. L. KEYFITZ, *The triple point paradox for the nonlinear wave system*, SIAM J. Appl. Math., 67 (2006), 321–336.

[20] A. M. TESDALL, R. SANDERS, AND B. L. KEYFITZ, *Self-similar solutions for the triple point paradox in gasdynamics*, SIAM J. Appl. Math., 68 (2008), 1360–1377.